**Supporting Information for:**

# Electron-Phonon Coupling and Resonant Relaxation from 1D and 1P States in PbS Quantum Dots

Eric R. Kennehan,[1] Grayson S. Doucette,[2,3] Ashley R. Marshall,[4,5] Christopher Grieco,[1] Kyle T. Munson,[1] Matthew C. Beard,[4] John B. Asbury[1]*

1. Department of Chemistry, The Pennsylvania State University, University Park, PA 16802, USA.
2. Intercollege Materials Science and Engineering Program, The Pennsylvania State University, University Park, PA 16802, USA.
3. Department of Materials Science and Engineering, The Pennsylvania State University, University Park, PA 16802, USA.
4. Chemical and Materials Science, National Renewable Energy Laboratory (NREL), Golden, CO 80401, USA.
5. Department of Chemistry and Biochemistry, University of Colorado, Boulder, CO 80309, USA.

**Table of Contents:**

**<u>Section 1</u>: Transient absorption spectroscopy for oleate capped colloidal solutions and $I^-$ /MPA capped films of PbS QDs.**

Broadband transient absorption (TA) spectroscopy was performed on solutions of oleate capped solutions and $I^-$/MPA capped PbS quantum dot (QD) films in addition to oleate capped films, to determine the effects of substrates or ligands on the measured electronic transitions. Spectra for these samples collected at 20 ns are shown in **Figures S1**-**S2**. The excited state absorption (ESA) portion of the TA data was able to be fit with the sum of two positive log-normal distribution functions while a single log-normal function was used to fit the ground state bleach (GSB). The component functions and the total fit function are included in for all QD sizes measured in **Figures S1** and **S2** in order to highlight the robustness of the fitting protocol. Functions used to fit these data sets were similar to the functions used in fitting the TA spectra in **Figure 1** in the main text with slightly different energy, variance, and intensity values. The two ESA absorption features in the TA spectra were assigned to the $1S_{e(h)}$-$1P_{e(h)}$ and $1S_{e(h)}$-$1D_{e(h)}$ intraband transitions and the center frequencies (energies) of our fits were used to describe the transitions in the following discussions.

On the low energy side of the bleach a small absorption feature is present which we attributed to the linear Stark effect. This slight positive feature caused additional error in fitting the GSB. To account for this additional signal, the GSBs in **Figures S1 and S2** have been fit to log-normal functions, emphasizing the lineshapes on the high energy side of the bleach to reproducibly estimate center frequency, intensity and variance. More accurate analysis is possible by modeling a fourth curve to fit the TA spectra, however this added complexity was unnecessary. We instead included and propagated the error associated with our fitting routine throughout the

data set and used the Visible to near-IR (Vis-NIR) absorption spectra wherever possible to more accurately represent optical bandgap.

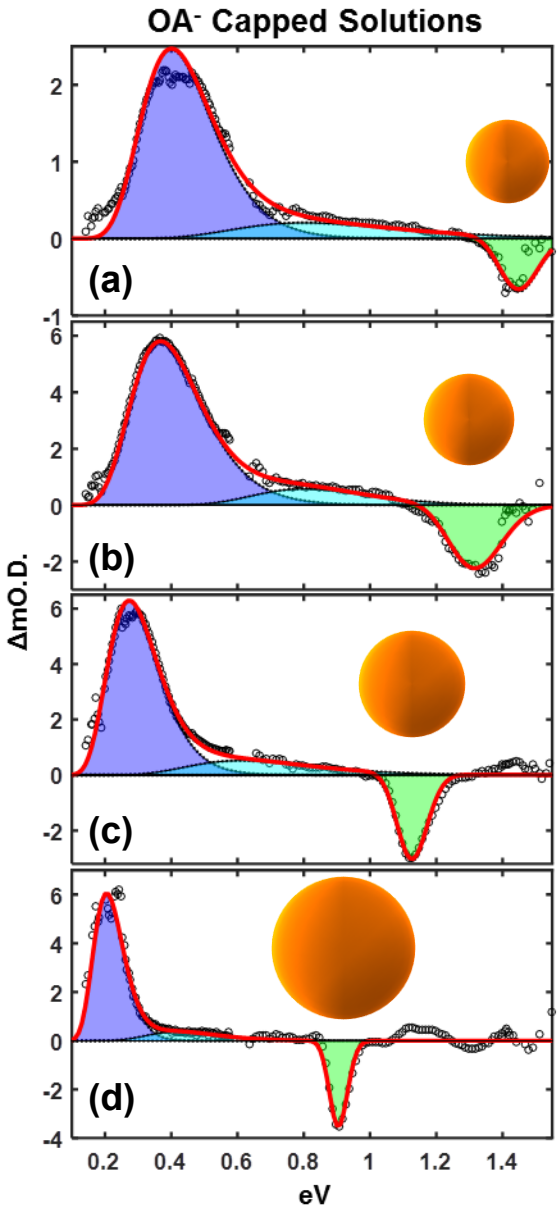


**Figure S1**. Transient absorption spectra of colloidal solutions of PbS QDs capped with oleate ligands at 20 ns for **(a)** 2.9 nm, **(b)** 3.1 nm, **(c)** 3.7 nm, and **(d)** 4.9 nm diameter dots. Red lines show the fit to the data using the sum of three log-normal functions representing the $1S_{e(h)}$-$1P_{e(h)}$ (violet) and $1S_{e(h)}$-$1D_{e(h)}$ (cyan) transitions, along with the bleach (green). Orange spheres represent the diameter of the QDs.

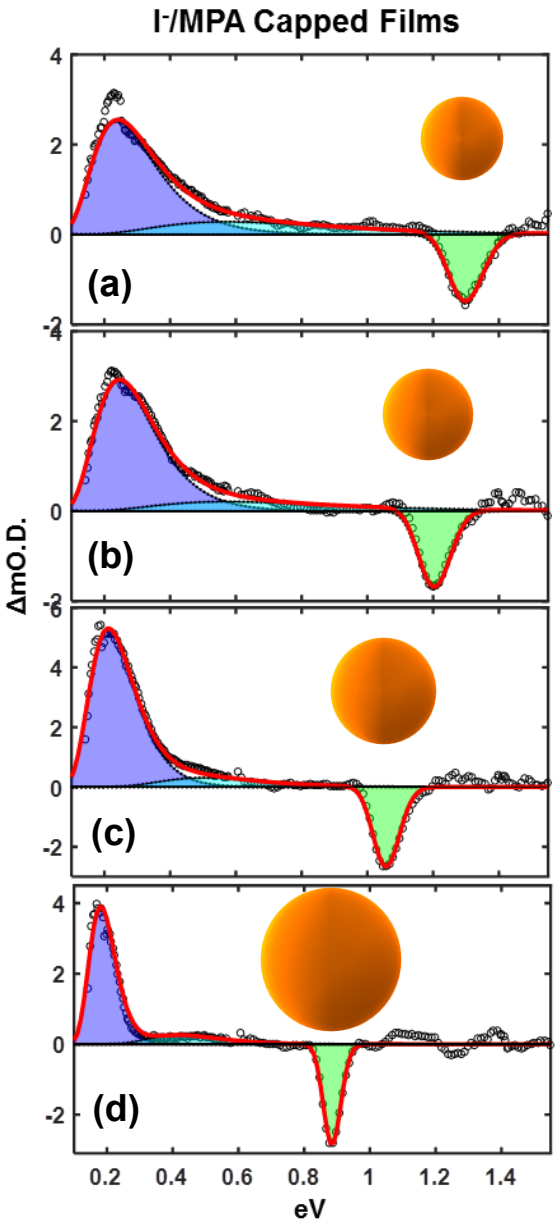


**Figure S2**. Transient absorption spectra of PbS QD films capped with $I^-$/MPA ligands at 20 ns for **(a)** 2.9 nm, **(b)** 3.1 nm, **(c)** 3.7 nm, and **(d)** 4.9 nm diameter dots. Red lines show the fit to the data using the sum of three log-normal functions representing the $1S_{e(h)}$-$1P_{e(h)}$ (violet) and $1S_{e(h)}$-$1D_{e(h)}$ (cyan) transitions, along with the bleach (green). Orange spheres represent the diameter of the QDs.

**Section 2: Characterization of QD size and first excitonic transitions.**

Vis-NIR absorption spectroscopy was performed on PbS QD films and colloidal solutions with native oleate ligands, as well as films that had been passivated with $I^-$/MPA ligands and are shown in **Figure S3** for the four dirfferent size QDs used in this study. The absorption spectra show clear first excitonic transitions that are characteristic of quantum confined nanoparticles.[1] Fitting the spectra using log-normal distributions allowed us to determine the approximate size of the dots through comparison of sizing curves calculated using the K•P four band envelope method.[2] The film absorption spectra have large etalons which are caused by sample reflectivity, yet distinct first excitonic transitions are still able to be fit well using log-normal distributions. We chose to use the center frequency of the log-normal distributions used to fit the first excitonic transition in colloidal solutions with oleate ligands to calculate representative dot sizes for our sample set since these solutions had the lowest probability of interdot electronic coupling. Interdot coupling is apparent in $I^-$/MPA ligand exchanged films which exhibited a strong red-shift, when compared to the oleate capped films and solutions[3-4] The colloidal solutions of PbS QDs with oleate ligands yielded dot diameters of 2.9 nm, 3.1 nm, 3.7 nm, and 4.9 nm which we use for the remainder of our discussions. Error in each of these diameters was found to be 0.1 nm, from the uncertainty associated with fitting the absorption spectra along the x-energy axis.

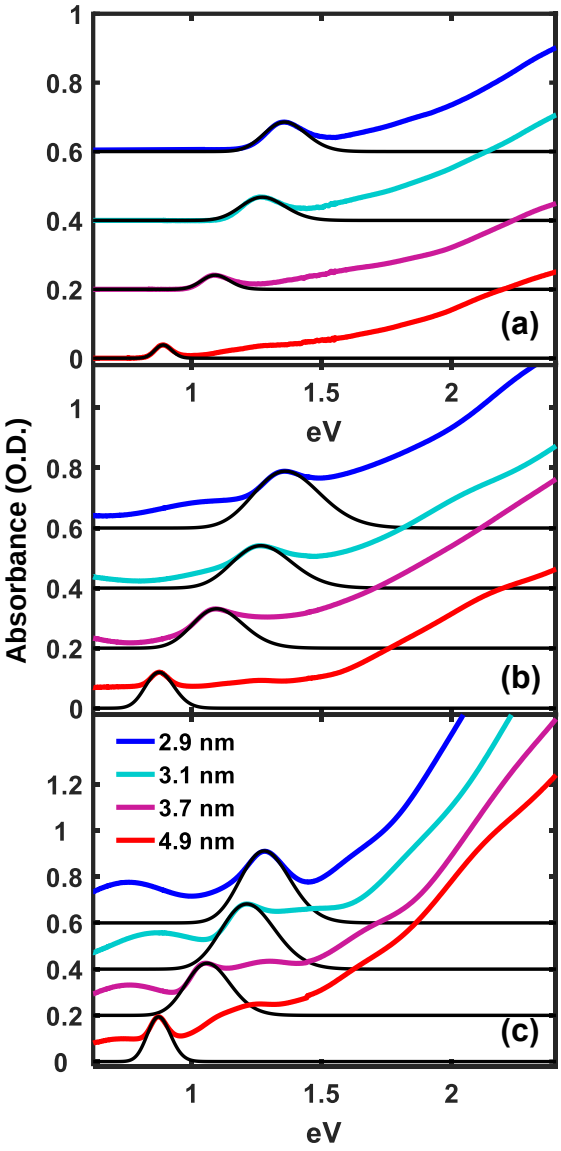


**Figure S3**. Vis-NIR absorption spectra of **(a)** colloidal PbS QD solutions capped with oleate and suspended in chloroform, **(b)** oleate capped, and **(c)** $I^-$/MPA capped PbS QD films. Corresponding log-normal fits to each absorption spectrum are shown for reference. Spectra for the various size dots are offset by 0.2 O.D. for clarity.

Colloidal PbS QD solutions with oleate ligands were drop-cast onto carbon grids and high resolution, transmission electron microscopy (TEM) was performed. The same solutions used for colloidal suspension measurements were used for the TEM images. The TEM images were collected on a FEI, Talos F200X with an XFEG source at 200 kV. **Figure S4** shows the TEM images for the four sizes of QDs used throughout the paper. The diameter of the dots was calculated to be 2.9 ± 0.3 nm, 3.1 ± 0.3 nm, 3.7 ± 0.4 nm,and 4.9 ± 0.4 nm, in agreement with the diameters calcualted from fitting the visible to near-IR absorption spectra. The TEM images illustrate that the QDs are not agglomerating which would indicate that ligands may be detaching from the surface.

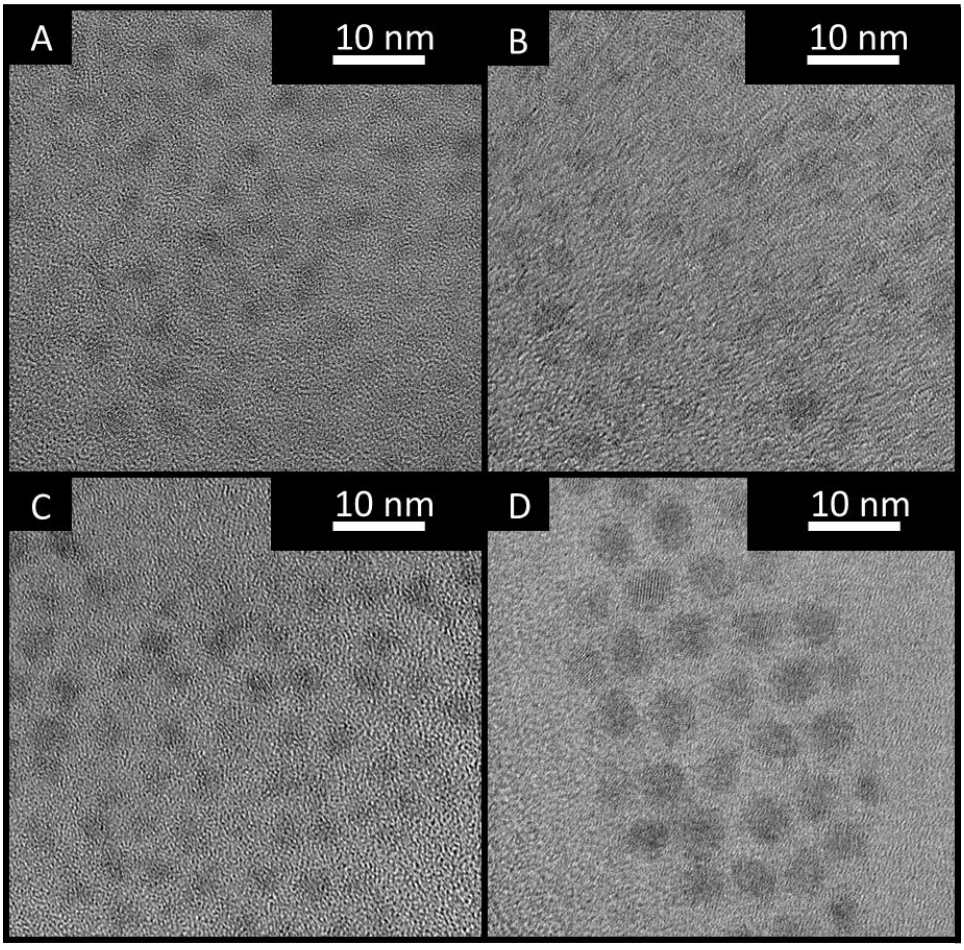


**Figure S4**.TEM images for **(a)** 2.9 ± 0.3 nm, **(b)** 3.1 ± 3nm, **(c)** 3.7 ± 0.4 nm, and **(d)** 4.9 ± 0.4 nm PbS QDs

**Section 3: Modeling 2.9 nm oleate capped PbS film transient absorption spectrum.**

On the low energy side of the bleach, a small absorption feature is present which does not fit the sum of the three log-normal distributions used to fit our data and additionally skews the GSB giving rise to a second derivative-like lineshape. One possible explanation for such a feature is a temperature dependent shift of the band edge and consequently the GSB. Such "thermal artifacts" have been characterized in detail previously.[5] Due to the low absorbed energy densities (<20 uJ/cm$^2$) that were used throughout our experiments, sample temperatures could not have exceeded a few kelvin above kT and so a thermal signatures were unlikely. However, to positively rule out a thermal signature, we performed temperature dependent Vis-NIR absorption spectroscopy. The temperature dependent data is shown in **Figure S5**. The bandgap of the PbS QD film with oleate ligands, blue-shifts with increasing temperature giving rise to a difference spectrum that is opposite to the trend observed in the TA data. Since the bangap shift in the opposite direction, we ruled out a thermal artifact from being present in our data.

Similar positive signatures have been measured in the TA spectra of PbS QDs near the GSB. These signatures have been attributed to biexciton, trions or a linear Stark effect. Biexcitons and Trions rapidly recombine on picoseconds or faster timescales.[6-8] Because our TA measurements take place on the nanosecond timescale, we attribute the induced absorption feature on the low energy side of the GSB to be caused by the linear Stark effect, which occurs as a result of the variation in the QD electric field when excited. The assignment of this positive feature is consistent with previous work.[9-10]

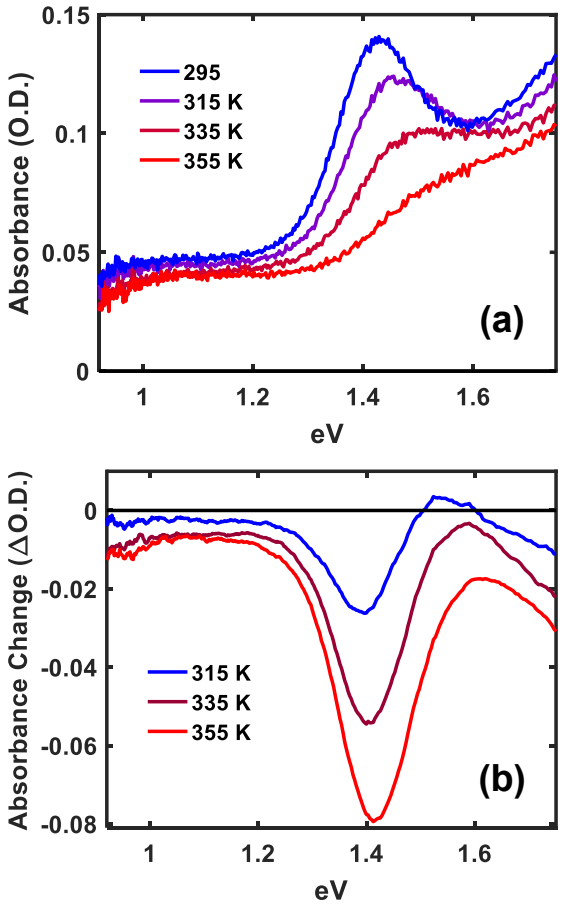


**Figure S5**. **(a)** Temperature dependent Vis-NIR absorption spectra of colloidal PbS QD films capped with native oleate ligands and **(b)** difference spectra from kT.

The TA spectra presented in **Figures 1**, **S1**, and **S2** were all fit using the sum of three log-normal distributions. One of these functions was used to fit the GSB in the same manner as the absorption spectra were all fit. The other two functions were necessary to fit the mid- to near-IR ESA feature and we assigned the significance of these functions to the $1S_{e(h)}$-$1P_{e(h)}$ and $1S_{e(h)}$-$1D_{e(h)}$ transitions. This model was chosen since the data could not be fit using a single asymmetric function, nor could it be fit using other simple, multi-function models. In **Figure S6**, we present the best possible fits for various functions to demonstrate the poor quality of the fits for models

we disregarded along with our reasoning for selection the sum of two log-normal distributions as the correct model for our data.

**Figures S6a**, **S6c**, and **S6e** correspond to a single log-normal, skew-normal, and Gaussian function, respectively. These functions very clearly do not fit the data, and can be readily eliminated as appropriate models for our data. **Figure S6b** shows the sum of two log-normal functions and is included as a comparison since this model was chosen to represent our data due to the quality of the fit and the application to a physical model. In **Figure S6d** we demonstrate the best fit for the sum of two skew-normal distributions. The quality of the fit is quite good, although the function does not fit the data as well as the log-normal functions. In addition to having a slightly different curvature, skew-normal distributions are not know to have physical relevance to colloidal systems, whereas log-normal functions are used to describe a size independent growth process as in the case for our QDs. For this reason we eliminated the two skew-normal functions as the correct fit to our data. Using the sum of two Gaussian functions (**Figure S6f)** we obtain a fit which does not fit the data well. In addition, the higher energy Gaussian function must extend below 0 eV in order to fit the broad curvature of the high energy transition. A negative difference in energy between initial and final states is irrelevant, and we concluded that two Gaussians were not a suitable model. **Figure S6g** shows the sum of three Gaussian functions to represent the data. We are able to fit the data quite accurately using three Gaussian functions, however the quality of the fit is not any greater than that for the sum of two log-normal distributions. Since fitting the data with three Gaussians is more complex than fitting with the sum of two log-normal distributions, without improving the fit quality, we chose the log-normal functions. In addition to requiring the fewest number of functions to accurately represent the data, log-normal distributions have physical relevance in colloidal sciences.

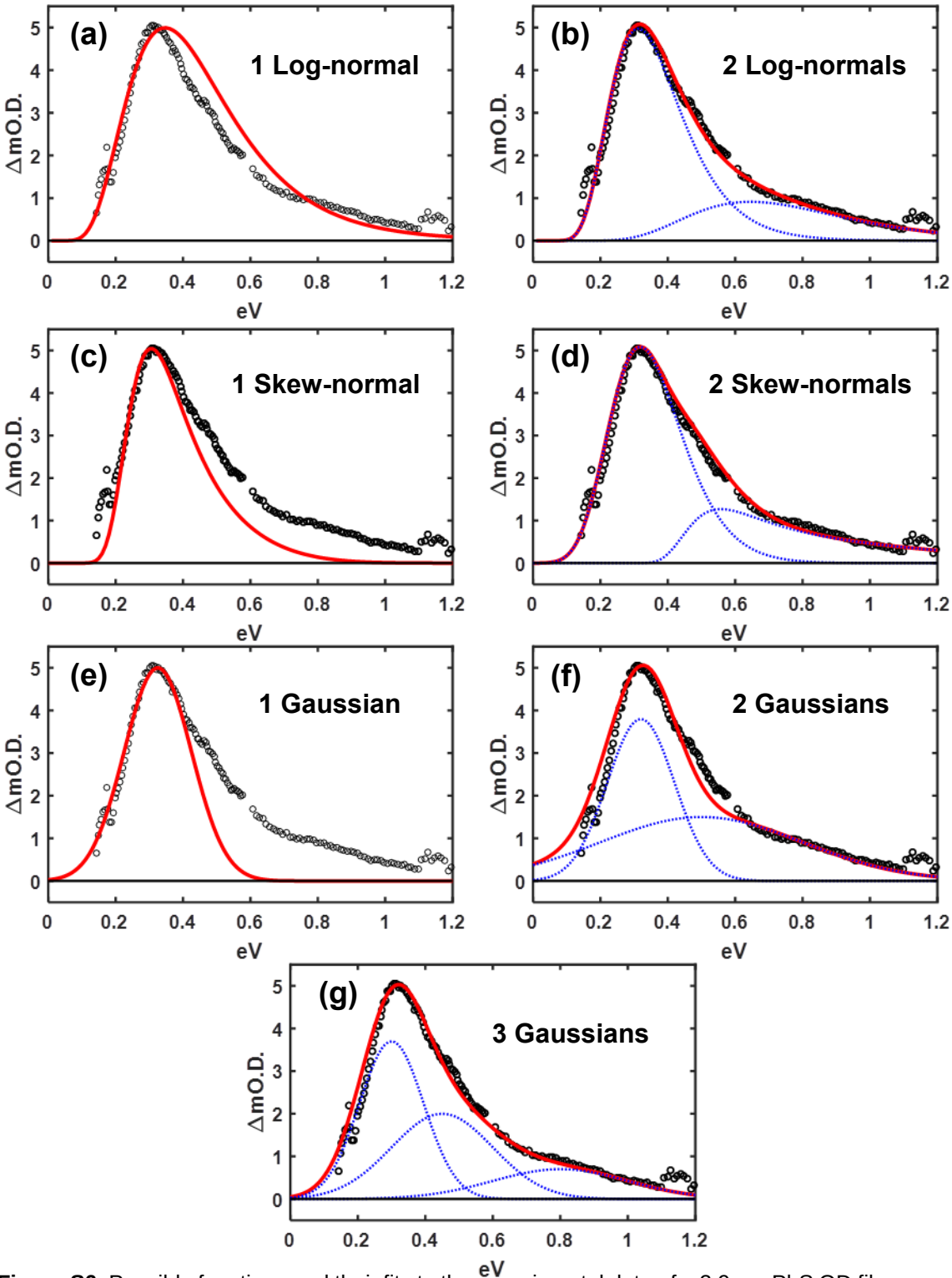


**Figure S6**. Possible functions and their fits to the experimental data of a 2.9 nm PbS QD film capped with oleate ligands with **(a)** 1 log-normal distribution, **(b)** sum of 2 log-normal distributions, **(c)** 1 skew-normal distribution, **(d)** sum of 2 skew-normal distributions, **(e)** 1 Gaussian function, **(f)** sum of 2 Gaussian functions, and **(g)** sum of 3 Gaussian functions.

**Section 4: Time-evolution of PbS QD TA spectra showing the absence of spectral evolution.**

Time-resolved transient absorption measurements were conducted on oleate capped films, colloidal solutions and I⁻/MPA films of PbS QDs. **Figures S7-S9** demonstrate the time-evolution of the spectra, in which the overall shape of the spectra is unchanged over the entire excited state lifetime. Using the same log-normal distributions that were used to fit our spectra at 20 ns and modifying only intensity, the TA spectra at every time slice are able to be accurately modeled. This clear fitting method is demonstrated for a 2.9 nm PbS QD film capped with oleate ligands in in **Figure S10**.

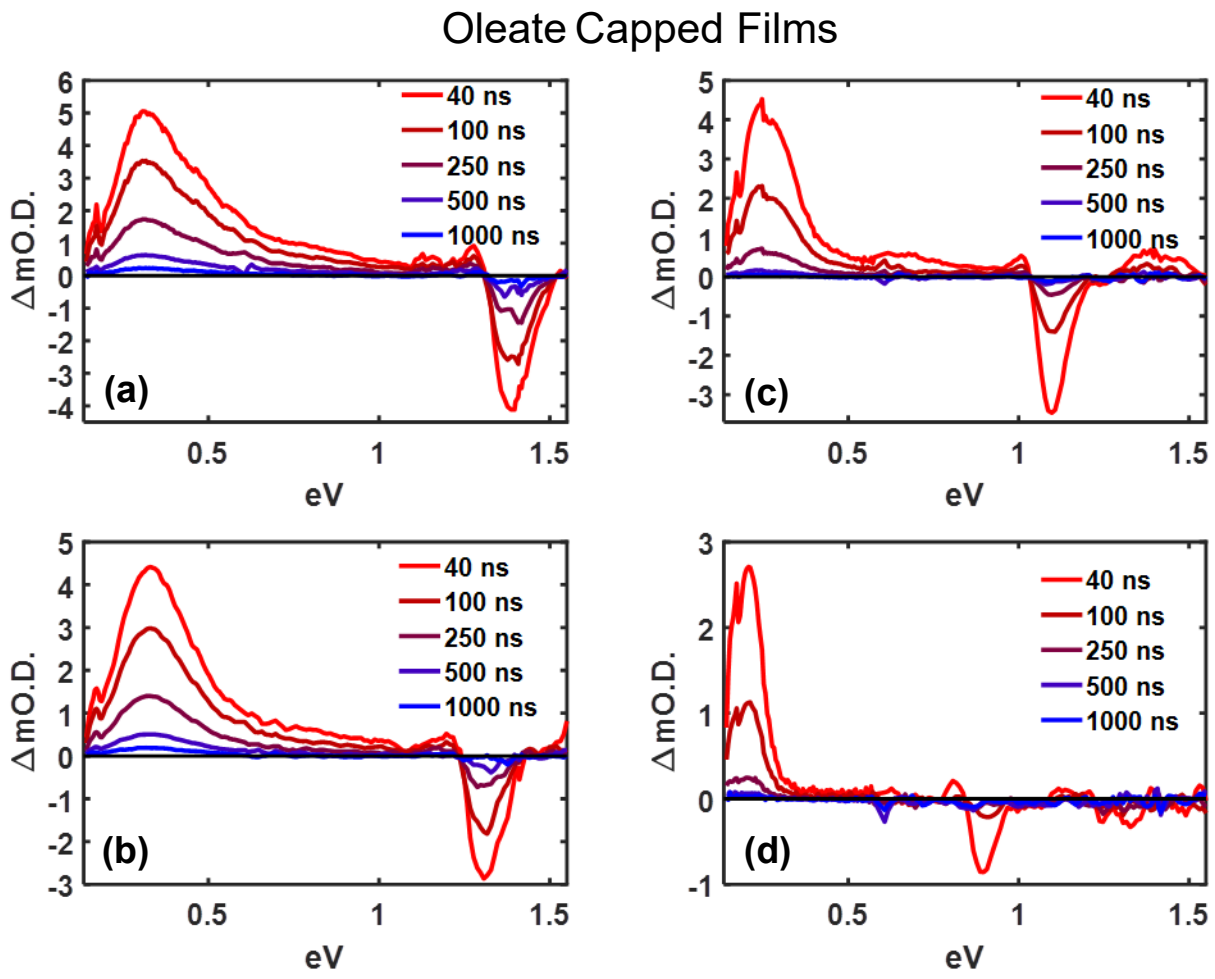


**Figure S7**. Nanosecond, broadband transient absorption spectra of **(a)** 2.9 nm, **(b)** 3.1 nm, **(c)** 3.7 nm, and **(d)** 4.9 nm PbS QD films capped with oleate ligands taken at select time slices.

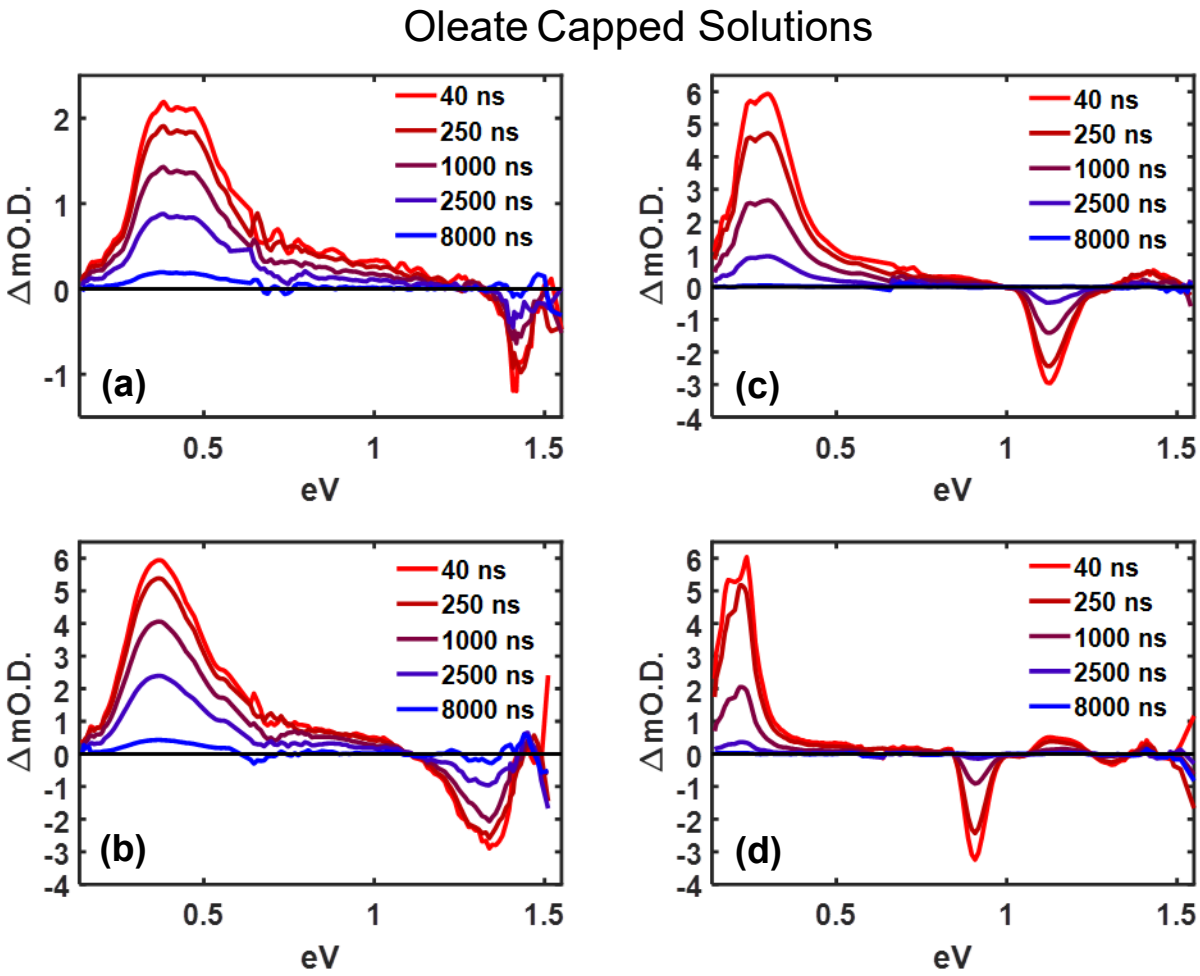


**Figure S8**. Nanosecond, broadband transient absorption spectra of **(a)** 2.9 nm, **(b)** 3.1 nm, **(c)** 3.7 nm, and **(d)** 4.9 nm PbS QD solutions capped with oleate ligands taken at select time slices.

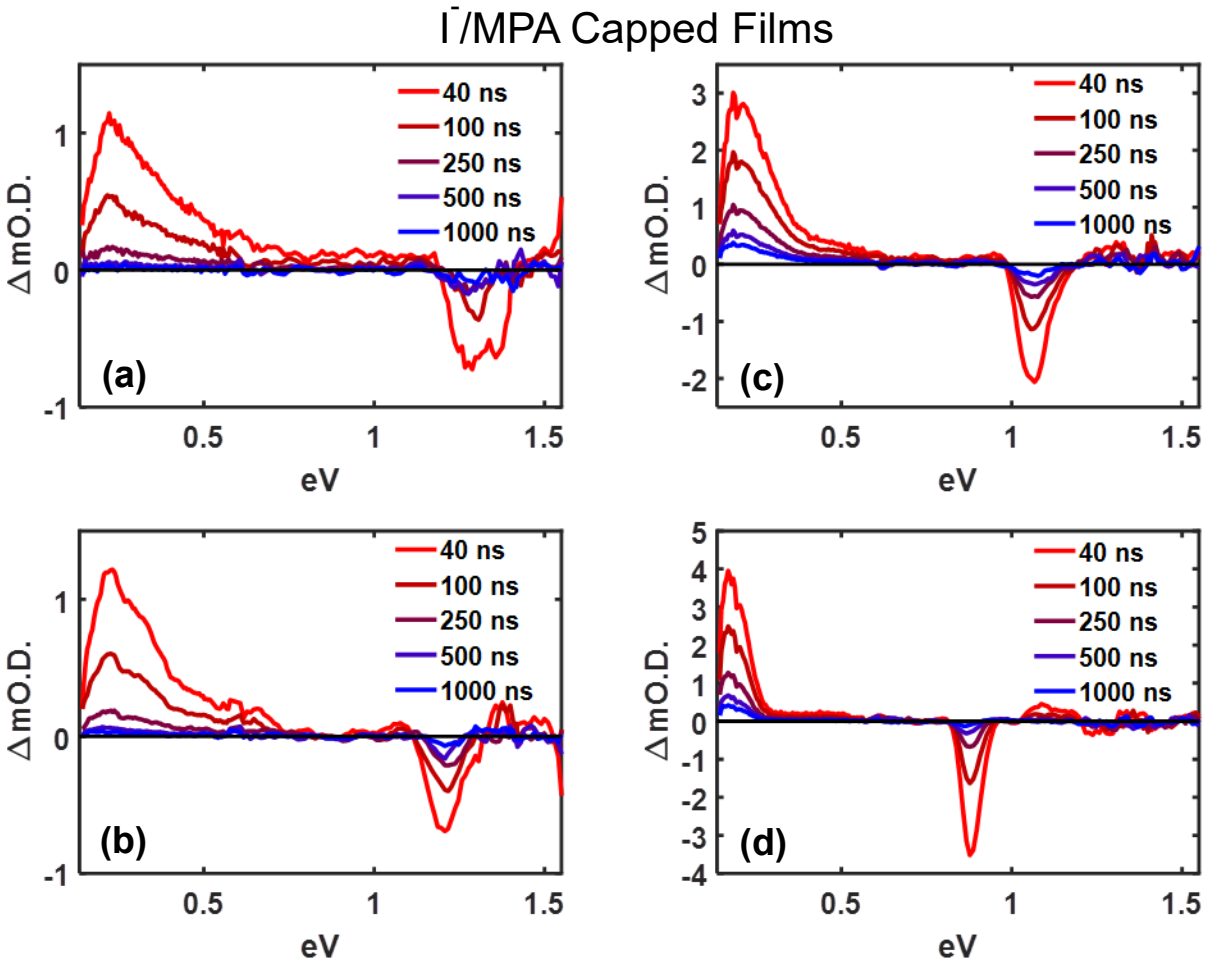


**Figure S9**. Nanosecond, broadband transient absorption spectra of **(a)** 2.9 nm, **(b)** 3.1 nm, **(c)** 3.7 nm, and **(d)** 4.9 nm PbS QD films capped with $I^-$/MPA ligands taken at select time slices.

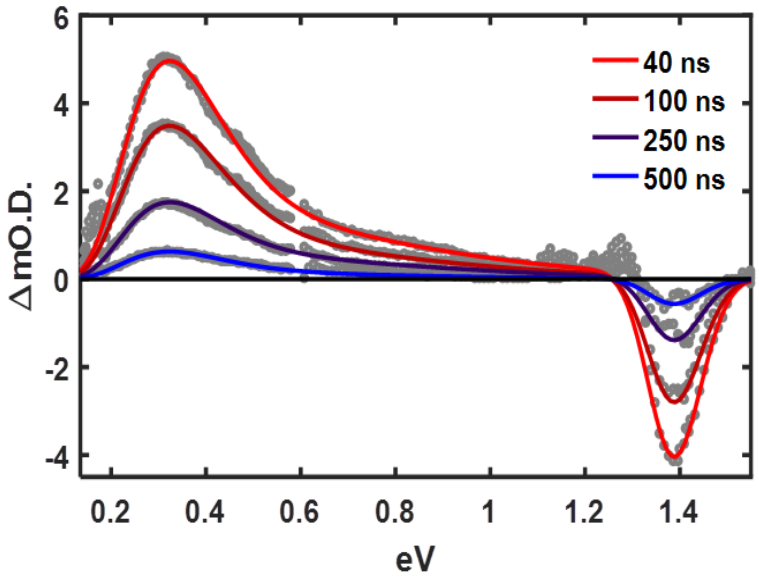


**Figure S10**. Nanosecond broadband transient absorption spectra for an oleate capped 2.9 nm PbS QD film with fits for multiple time slices using the sum of two positive and one negative log-normal distributions.

**Section 5: Kinetics comparison of transient absorption signatures with photoluminescence.**

Using our flash-photolysis spectrometer, we were able to time-resolve the complete ground state recovery of each component comprising the TA spectrum. We also took advantage of our setup to measure the integrated photoluminescence (PL) decay of the QD sample to compare the two. Analysis of the kinetics was particularly useful in assigning the low and high energy ESAs to the $1S_{e(h)}$-$1P_{e(h)}$ and $1S_{e(h)}$-$1D_{e(h)}$ transitions. All of the states that were assigned in the TA spectra have a common initial energy state, the $1S_{e(h)}$ state, and thus should all have matching kinetics for this assignment to hold true. **Figures S11-12**, demonstrates that in both of the oleate capped QD samples measured, the kinetic traces for the $1S_{e(h)}$-$1P_{e(h)}$ and $1S_{e(h)}$-$1D_{e(h)}$ match the recovery of the GSB, supporting the claim made in the paper. In addition, the PL lifetime also matches lifetime of the bleach recovery, within experimental error, eliminating the possibility that one of the transitions observed in the TA spectra is a defect state.

For $I^-$/MPA capped PbS QD films, the ESAs and the GSB are longer lived than the PL (**Figure S13**). This difference in the lifetimes for the TA and PL is likely a result of either trap states or the presence of free carriers in the films. Traps states mediate non-radiative recombination and could cause the bleach to outlive the radiative decay, similar to previous reports.[11] Previous reports have also shown that performing ligand exchange procedures in PbS QDs can result in imperfect passivation and the formation of trap states at the surface of the QD.[12-13] In addition to potential defect-states, free carriers may be present in these films. These films were specifically chosen due to their photovoltaic efficiency and are known to be electronically coupled resulting in exciton separation into free carriers.[3-4, 14] Free carriers can also recombine nonradiatively and can explain the change in the decay kinetics from exponential in the oleate samples to a power law in the $I^-$/MPA films. Such power law relaxation dynamics are expected for bimolecular processes,

such as free carrier recombination and highly suggests that the samples are separating excitons.[11] Whether trap states or free carriers are present in the $I^-$/MPA films, the TA spectra is consistent with oleate capped samples and therefore are technique is not sensitive to these species in this experiment.

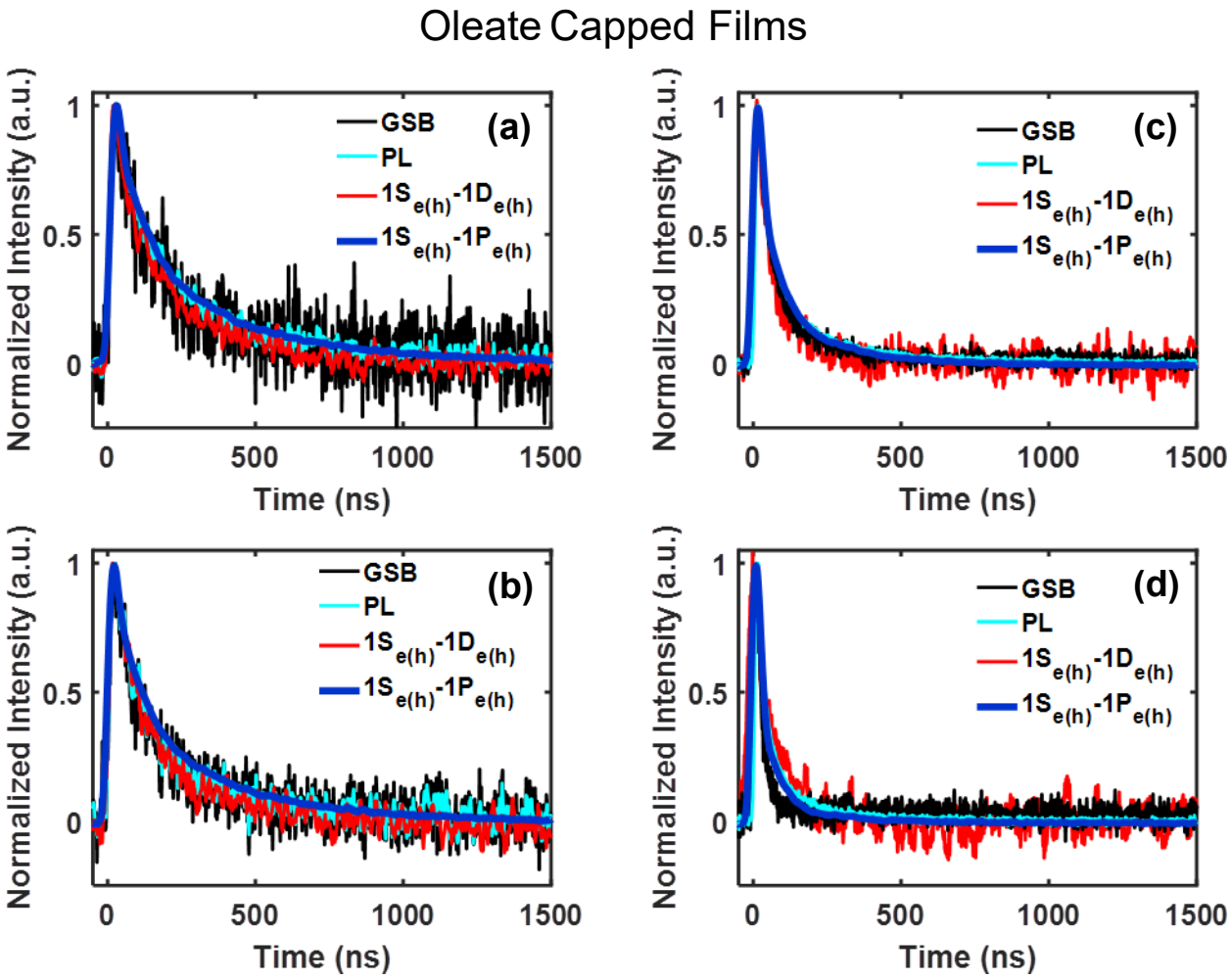


**Figure S11**. Transient absorption kinetics for each measured TA transition and PL decays for **(a)** 2.9 nm, **(b)** 3.1 nm, **(c)** 3.7 nm, and **(d)** 4.9 nm PbS QD films capped with oleate ligands.

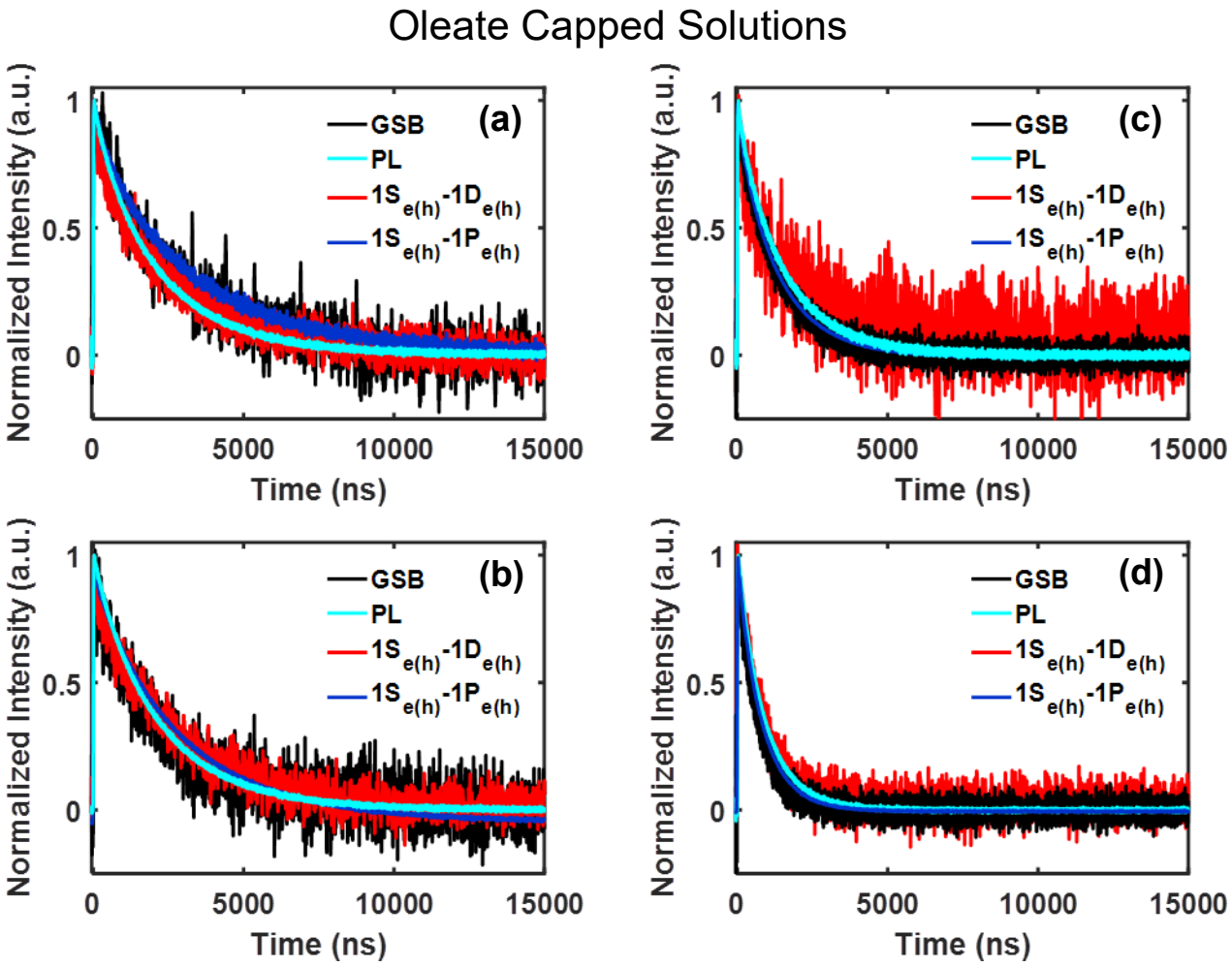


**Figure S12**. Transient absorption kinetics for each measured TA transition and PL decays for **(a)** 2.9 nm, **(b)** 3.1 nm, **(c)** 3.7 nm, and **(d)** 4.9 nm PbS QD solutions capped with oleate ligands.

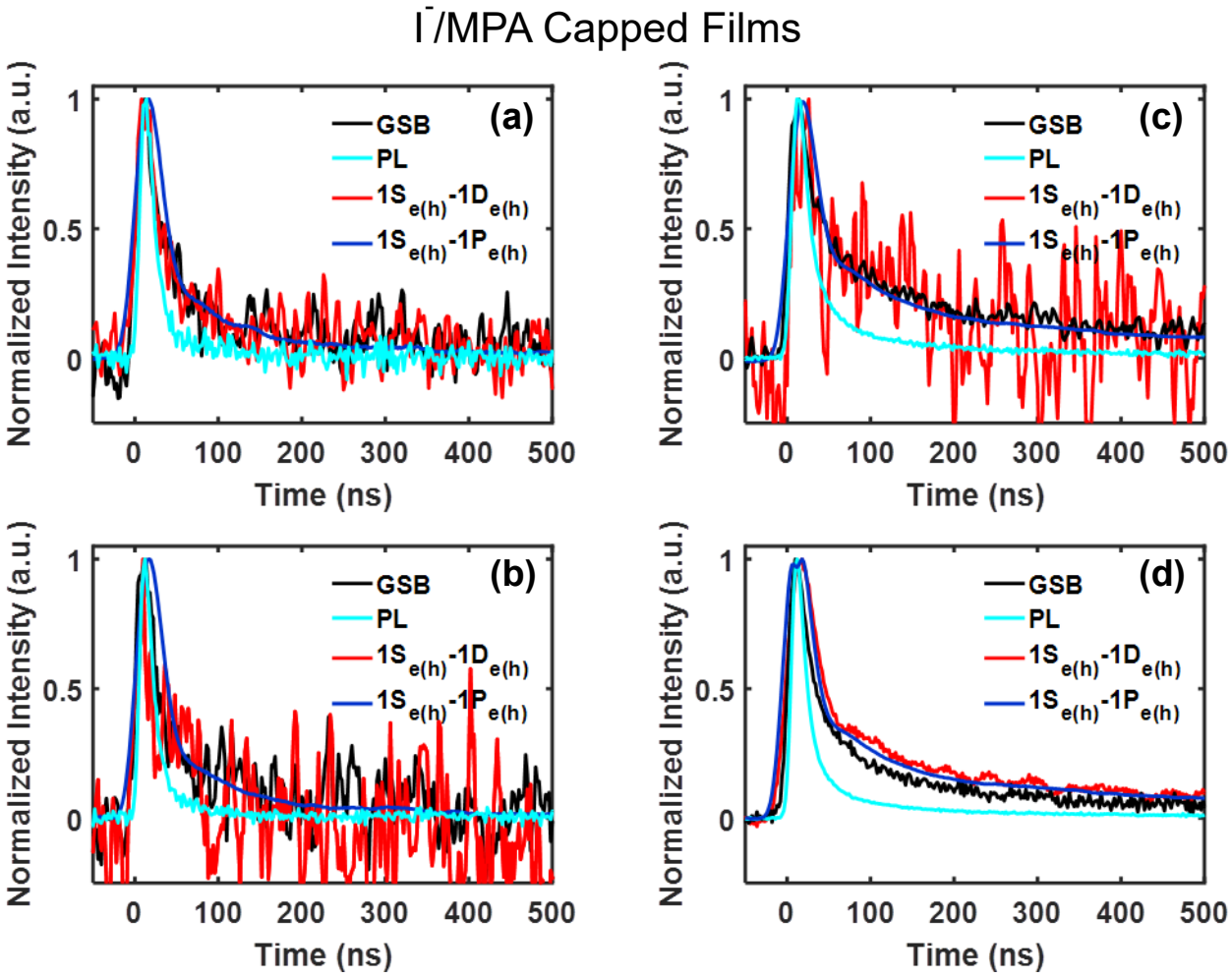


**Figure S13**. Transient absorption kinetics for each measured TA transition and PL decays for **(a)** 2.9 nm, **(b)** 3.1 nm, **(c)** 3.7 nm, and **(d)** 4.9 nm PbS QD solutions capped with $I^-$/MPA ligands.

**<u>Section 6</u>: Comparison of measured $1S_{e(h)}$-$1P_{e(h)}$ and $1S_{e(h)}$-$1D_{e(h)}$ transitions to predicted energies from the K•P model.**

The final method used to identify the low energy and high energy transitions as the $1S_{e(h)}$-$1P_{e(h)}$ and $1S_{e(h)}$-$1D_{e(h)}$ was comparing the measured transition energies to the calculated energies predicted from the K•P four band envelope function model. **Figure S14** shows the measured transition energies plotted with the predicted energies as a function of the first excitonic transition (optical bandgap). The measured transition energies quantitatively agree with the calculated energies within experimental error for oleate solutions and $I^-$/MPA films. Due to the spectral breadth of the ESA features and the small energy separation between predicted electron and hole specific transitions, we are unable to identify which transition we are observing or if we have contributions from both states. We use $1S_{e(h)}$-$1P_{e(h)}$ and $1S_{e(h)}$-$1D_{e(h)}$ to denote all four of the possible transitions represented by the dashed and solid lines **in Figure S14**.

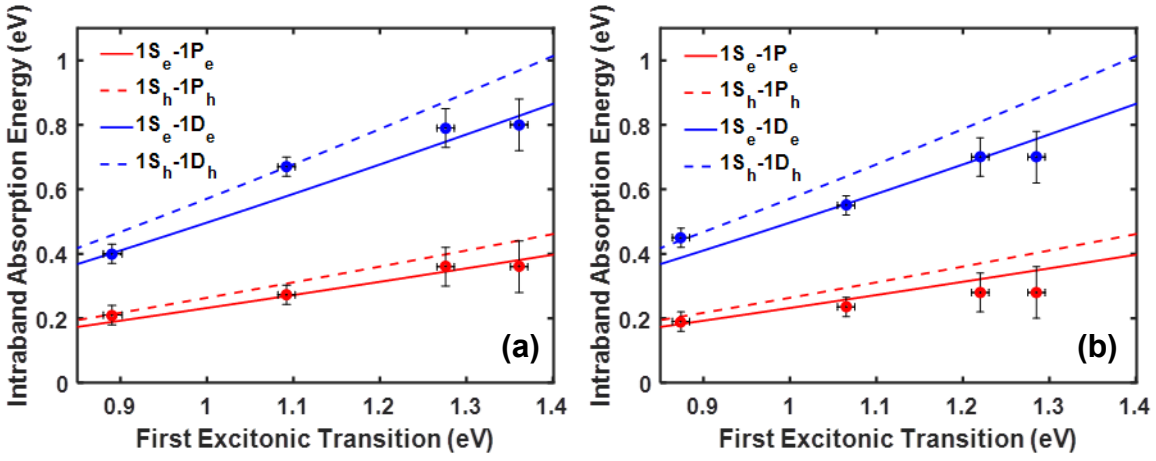


**Figure S14**. Measured intraband transition energies for **(a)** oleate capped colloidal solutions and **(b)** $I^-$/MPA capped films of PbS QDs with their optical bandgaps compared to calculated $1S_{e/h}$-$1P_{e/h}$ and $1S_{e/h}$-$1D_{e/h}$ transition energies using the K•P method.

**Section 7: Temperature dependent transient absorption experiments.**

As an alternate explanation for the observation of the formally forbidden $1S_{e(h)}$-$1D_{e(h)}$ transition in the transient absorption spectra, we considered the possibility that the transition was allowed due to an indirect transition involving intervalley scattering of phonons within the conduction band.[2] We undertook a temperature dependent study of the transient absorption spectra to investigate whether the intraband $1S_{e(h)}$-$1D_{e(h)}$ transition was allowed due to coupling to excited phonons. We reasoned that by eliminating the number of thermally excited phonons at lower temperature, the observed oscillator strengths of the $1S_{e(h)}$-$1D_{e(h)}$ transitions would be significantly reduced. **Figure S15** depicts transient absorption spectra measured under identical conditions to those depicted in **Figure 1** but at temperatures of 298 and 77 K. By performing TA experiments at 77 K, we eliminated nearly all of the vibrational modes measured in the resonant Raman and far infrared absorption spectra for PbS QDs.[15-17] Specifically, at such low temperatures, the available energy of the system (6.6 meV) was below the predicted energy of the X-point phonon mode (~10 meV) responsible for intervalley scattering from one L point in the valence band to another L point in the conduction band.[2] Despite a large reduction in the occupied phonon population, the amplitude of the measured $1S_{e(h)}$-$1D_{e(h)}$ transition in our QDs was unchanged when compared to the room temperature TA spectra. The fact that a significant difference in measured intensity and line shape of the $1S_{e(h)}$-$1D_{e(h)}$ transition was not observed for a significant change in density of excited phonon modes indicated that the transition was not the result of an indirect excitation. We note that a significant increase in the lifetimes of the GSB and ESAs at low temperatures was observed which may be attributed to shallow trapping below the band edge in the sample (**Figure S16**). These results suggested that the transition was a direct absorption event and supported the claim that the transition originated from a breakdown of parity selection rules within the QD.

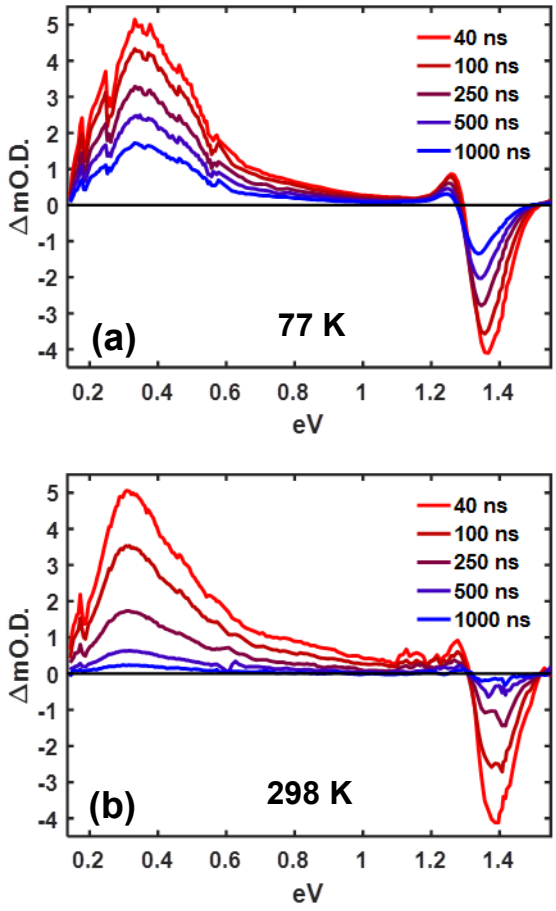


**Figure S15**. Broadband transient absorption spectra of an oleate capped PbS QD film at **(a)** 77 K and **(b)** 298 K.

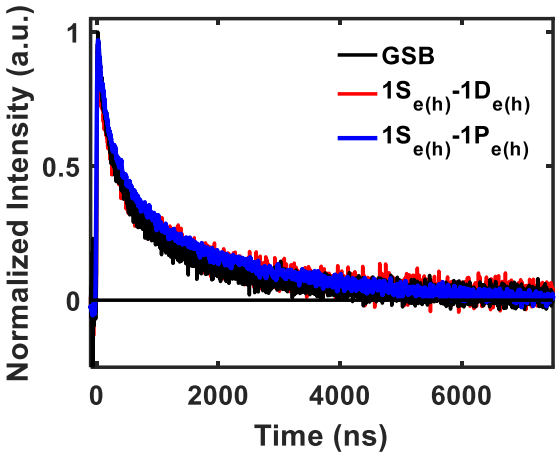


**Figure S16**. Normalized transient absorption kinetics for the GSB, $1S_{e(h)}$-$1P_{e(h)}$, and $1S_{e(h)}$-$1P_{e(h)}$ of the 2.9 nm oleate capped PbS QD film at 77 K.

**Section 8: Size dependent absorption strength of the intraband transitions.**

The $1S_{e(h)}$-$1D_{e(h)}$ transition if formally forbidden due to parity selection rules and so we sought to identify the cause for its strong absorption signature in our data. The low and high energy ESA features in the TA spectra of **Figures 1**, **S1**, and **S2** were observed to be highly dependent on nanocrystal size, with both transitions becoming narrower as the QD radius increases. Additionally, the intensity of the $1S_{e(h)}$-$1P_{e(h)}$ and $1S_{e(h)}$-$1D_{e(h)}$ transitions appeared to be shrinking with increasing dot size. To quantify this effect we investigated the relative oscillator strengths of the transitions, through their spectral area, to the volume of the QD. This comparison is shown in **Figure S17**. In **Figure S17**, the areas of the measured transitions have been normalized to the bleach. In normalizing in such a way, we took into account any size dependent differences in extinction, and normalize the excited state concentration. Additionally, normalizing in such a manner eliminates increased area of a transition due to inhomogenous broadening as a result of non-uniform QD size distributions in a sample. This procedure causes the bleach area to always be one and it has been included in the figures for reference. The $1S_{e(h)}$-$1D_{e(h)}$ transition is shown to increase as the QD volume decreases, while the $1S_{e(h)}$-$1P_{e(h)}$ transition has the opposite trend. This variation is characteristic of "oscillator strength borrowing" that can arise from coupled, nearly degenerate transitions that form a Fermi resonance[18] or from systems in which a break of symmetry allows a formally forbidden transition to become allowed. In the latter case, the break of symmetry can also suppress the oscillator strength of the normally symmetry allowed transition. A break in symmetry has been predicted to occur in PbS QDs[19] and such a break in symmetry is consistent with the strong size-dependence we observed in this study. We concluded that the $1S_{e(h)}$-$1D_{e(h)}$ transition becomes allowed due to a break in inversion symmetry in small QDs as the crystal lattice shifts away from the center of the nanocrystal.

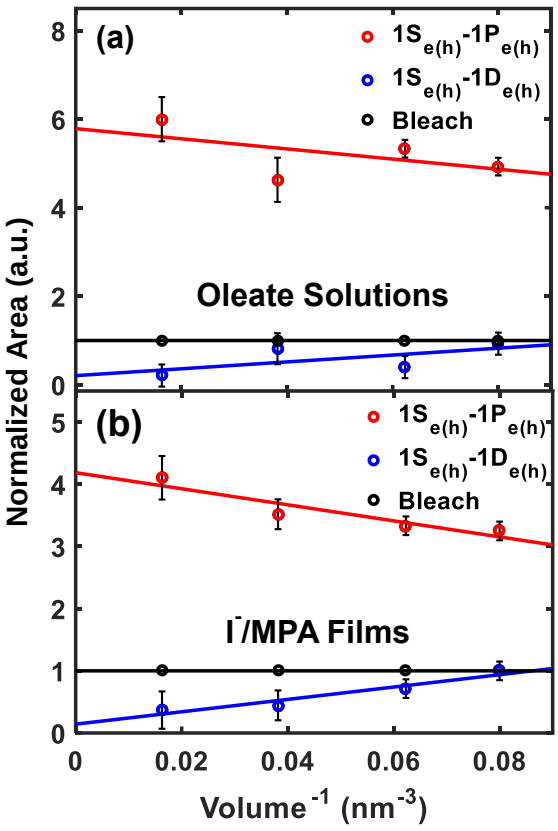


**Figure S17**. Area of log-normal fits to the transient absorption spectra at 20 ns, normalized to the area of the bleach for **(a)** oleate capped solutions and **(b)** $I^-$/MPA capped PbS QD films. Solid lines represent the line of best fit for the data points to emphasize trends.

**Section 9: Spectral linewidth dependence of measured electronic transitions on QD radius.**

Broadening of electronic transitions in semiconductor nanocrystals is controlled by homogenous and inhomogenous broadening. Inhomogenous broadening is largely regulated by the size distribution of QD samples while homogenous broadening has been presented to be dominated by electron-phonon interactions.[20-21] Quantum confined systems have been shown to exhibit strong size dependence on electron-phonon coupling.[20] To determine the strength of electron-phonon coupling in our samples, we chose to analyze the size-dependent variances of the functions used to fit the measured GSB ($1S_h$-$1S_e$), $1S_{e(h)}$-$1P_{e(h)}$, and $1S_{e(h)}$-$1D_{e(h)}$ transitions measured in TA experiments. **Figure 4** highlights the volume-dependent trend that the variance follows in our samples and is consistent with previous reports.[20]

The size-dependent variation of all three transitions were fit using a power law function, similar to previous measurements of the homogenous line broadening in CdSe QDs with the form $\Gamma(V) = bV^{-n}$, where V is the volume of the QD, the y-intercept, b, accounts for size independent factors contributing to linewidth, and the exponent n controls the size-dependent scaling of the linewidth.[20] The y-intercept of each transition in **Figure 4** were quantitatively different and revealed that higher energy states are more strongly coupled to vibrational modes in PbS QDs than lower energy states. We are aware that we are unable to subtract inhomogeneous broadening from our data, however since inhomogenous broadening remains constant in each sample, the quantitative difference in y-intercept supports the claim that higher energy states are more strongly coupled to phonon.

To predict the types of phonon-modes that our QD samples are coupling to, we sought to linearize the variance by plotting our data against $1/R^3$. Using the inverse dependence on radius allowed us to identify the types of phonon modes which were present. For acoustic phonon modes,

deformation-potential coupling would scale as 1/R while piezoelectric coupling would scale as $1/R^2$.[20, 22-23] A linear dependence on $1/R^3$ would suggest coupling to longitudinal optical modes is occurring according proportional to the square of the Fröhlich interaction coupling constant. Plots demonstrating the variances as a function of $1/R^3$ are shown in **Figure S18** for oleate capped films of PbS QDs.[20] Such scaling suggest that LO modes may be responsible for the electron-phonon coupling that we measured in our experiments. Due to experimental error however, we avoid a firm assignment of the phonon modes present.

Additional size-dependent variance plots for oleate capped colloidal solutions and PbS QD films passivated with $I^-$/MPA ligands. These plots are shown in **Figures S19-S20** and uphold the same trends discussed for the oleate capped films above.

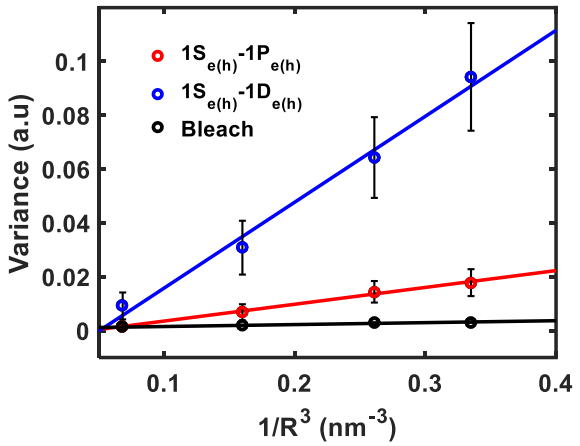


**Figure S18**. Variance of the $1S_{e(h)}$-$1P_{e(h)}$, $1S_{e(h)}$-$1D_{e(h),}$ and bleach transitions measured in TA spectra highlighting the dependence on $1/R^3$.

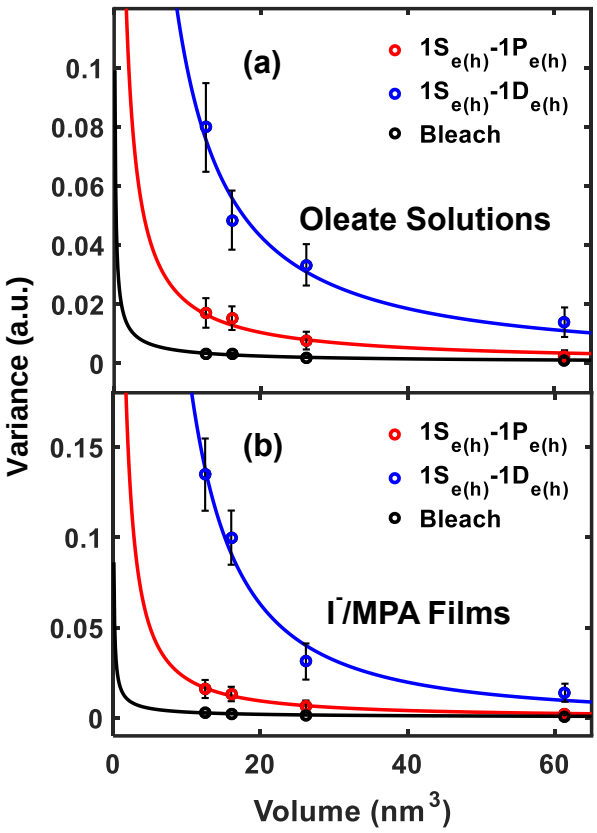


**Figure S19**. Variance of the $1S_{e(h)}$-$1P_{e(h)}$, $1S_{e(h)}$-$1D_{e(h)}$, and bleach features from the fits to the TA data for **(a)** oleate capped solutions, and **(b)** $I^-$/MPA capped PbS QD films.

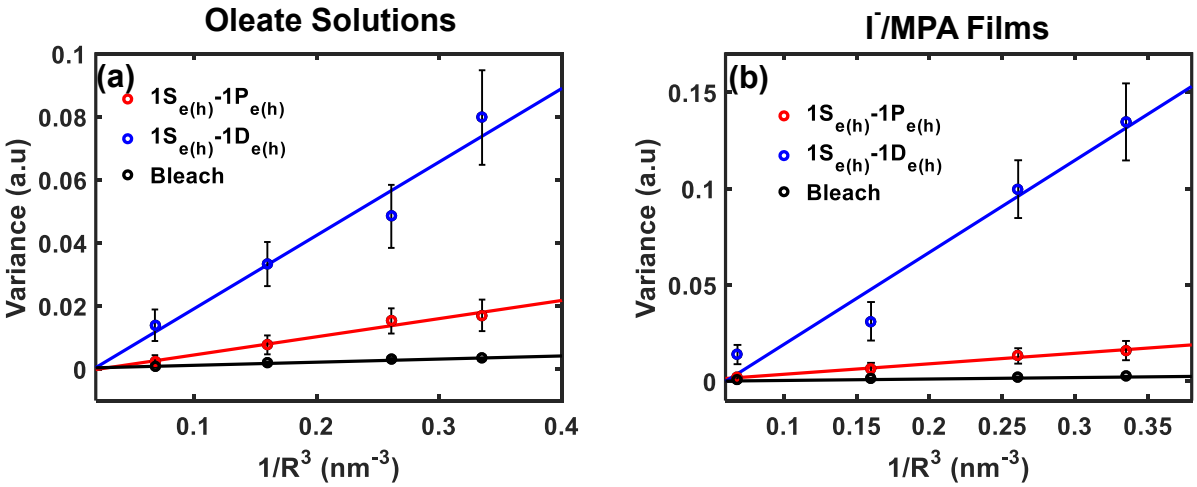


**Figure S20**. Variance of the $1S_{e(h)}$-$1P_{e(h)}$, $1S_{e(h)}$-$1D_{e(h)}$, and bleach transitions measured in TA spectra highlighting the dependencies on **(a)** oleate capped PbS solutions and **(b)** $I^-$/MPA capped films

**Section 10: Photoluminescence Spectra of QD films and solution.**

Transient photoluminescence spectra of all of the samples studied were measured in addition to transient absorption. The time-resolved spectra are given in **Figures S21-S23**. All samples had strong emission, with lifetimes depending on the radius and type of QD sample. Colloidal solutions with oleate ligands had the longest PL lifetimes while films capped with $I^-$ /MPA ligands had the shortest lifetime. The emission spectra also displayed a dynamic shift to lower frequency. This shift was likely a result of energy transfer to the largest diameter nanocrystals and was on the order of ~50 meV.

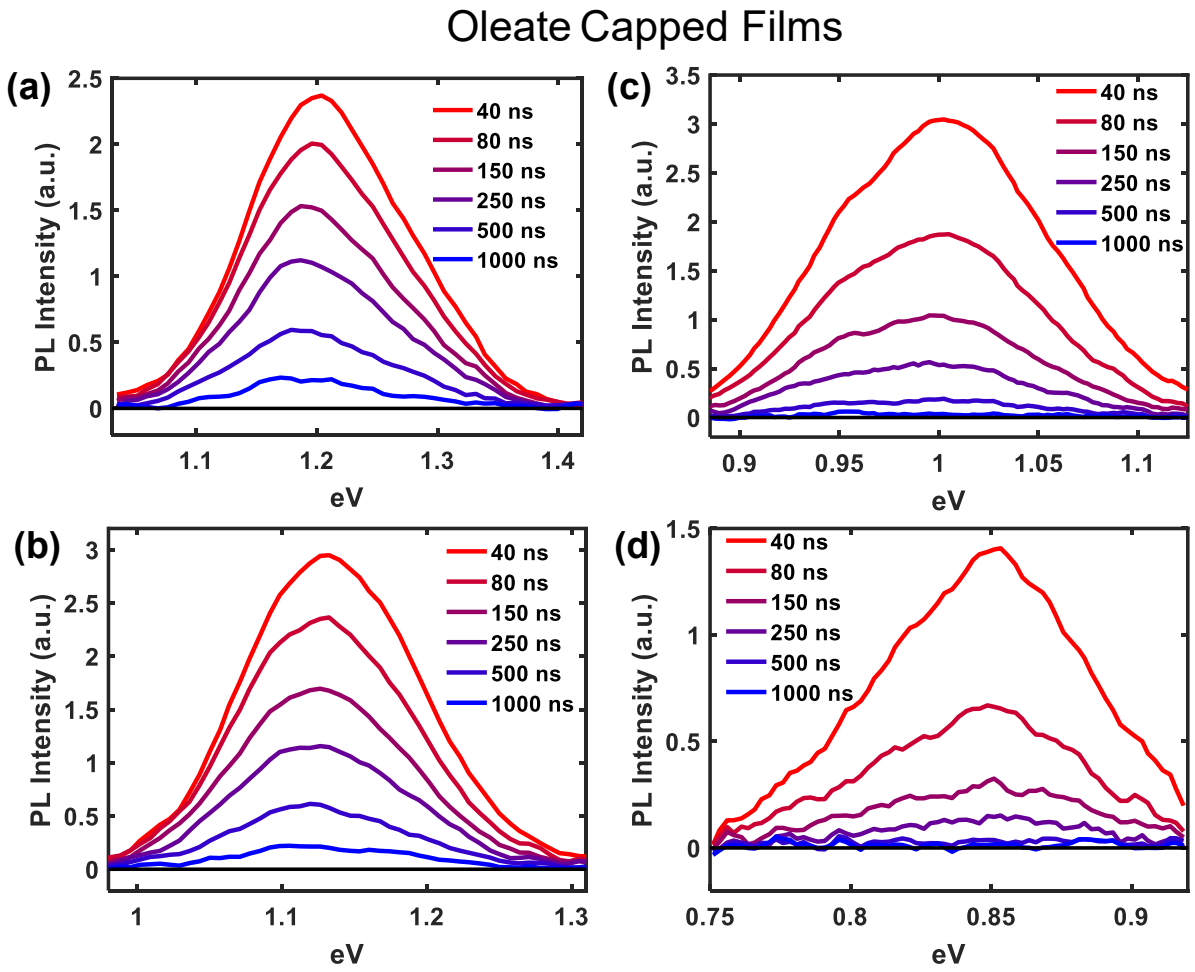


**Figure S21**. Photoluminescence decay traces for **(a)** 2.9 nm **, (b)** 3.1 nm, **(c)** 3.7 nm, and **(d)** 4.9 nm oleate capped PbS QD films.

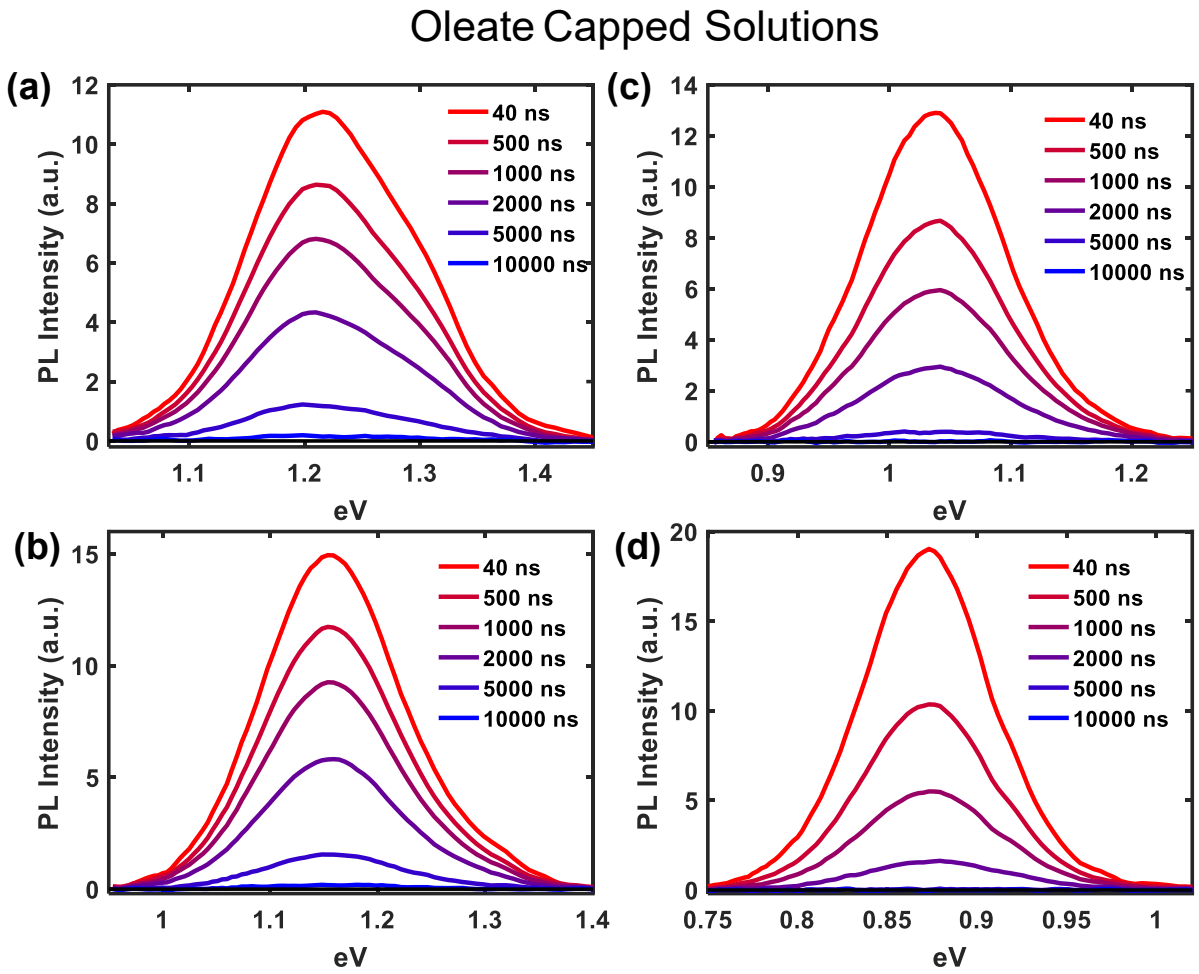


**Figure S22**. Photoluminescence decay traces for **(a)** 2.9 nm **, (b)** 3.1 nm, **(c)** 3.7 nm, and **(d)** 4.9 nm oleate capped, colloidal PbS QD solutions in chloroform.

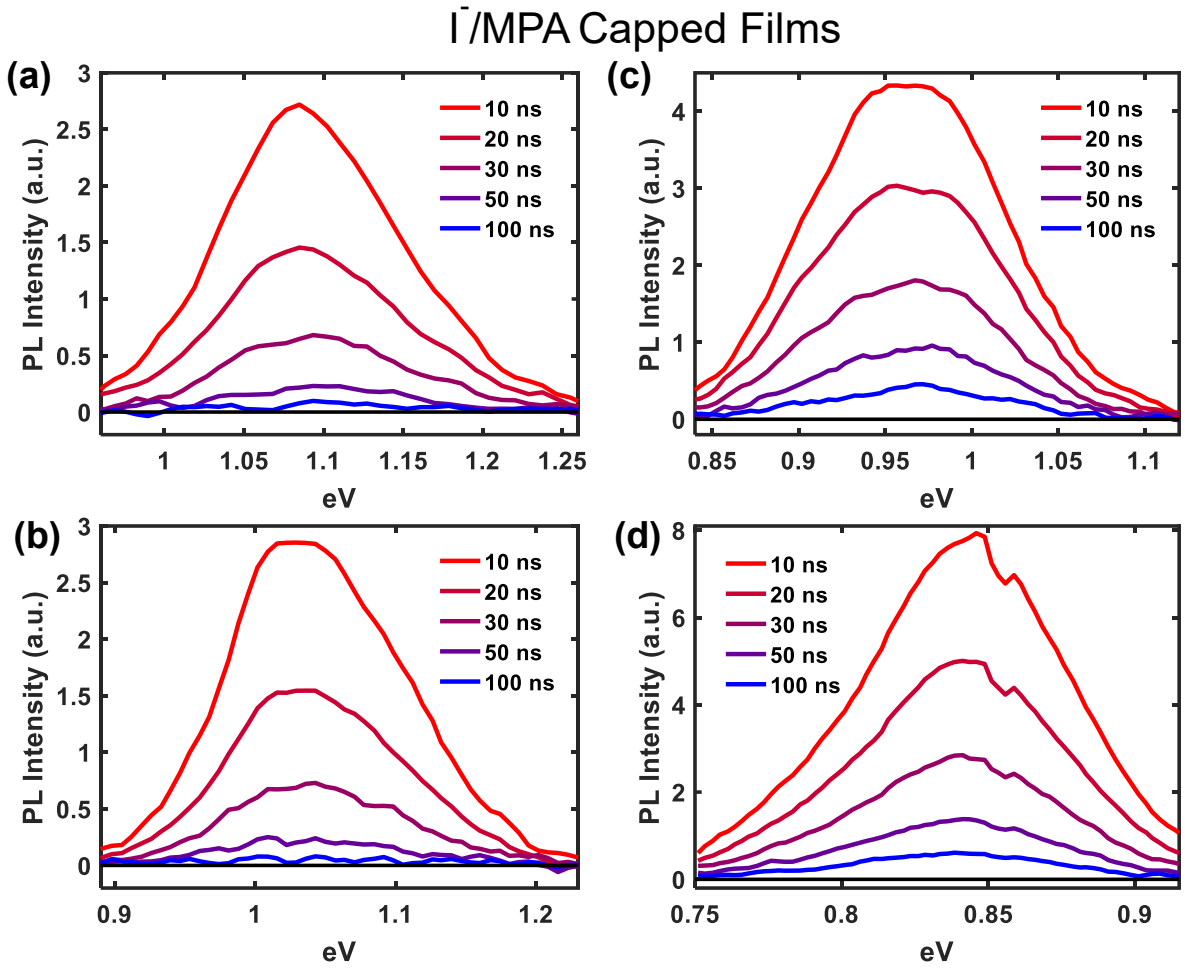


**Figure S23**. Photoluminescence decay traces for **(a)** 2.9 nm **, (b)** 3.1 nm, **(c)** 3.7 nm, and **(d)** 4.9 nm PbS QD films capped with $I^-$/MPA ligands.

**Section 11: Using transient absorption spectra as a measure of QD density of states**

Spectral density of state plots were constructed for colloidal PbS solutions capped with oleate ligands and thin films of $I^-$/MPA capped QDs. These plots are shown in **Figures S24-S25**. The plots exhibit identical, size dependent trends which were showcased in **Figure 5**. Small diameter QDs have increased spectral breadth that cause a large overlap area between the $1P_{e(h)}$ and $1D_{e(h)}$ states. In addition to a large overlap of the higher energy density of states, there is also an overlap of the $1S_{e(h)}$ and $1P_{e(h)}$ states. Such large spectral overlap is the direct result of electronic state coupling to vibrational modes. This energetic overlap provides resonant relaxation pathways between high energy states to the band edge. Through this mechanism, carriers are able to thermalize rapidly, approaching bulk cooling rates. Large diameter QDs maintain spectral overlap between $1D_{e(h)}$ and $1P_{e(h)}$ states, yet this overlap is reduced as the magnitude of electron-phonon coupling decreases. The $1S_{e(h)}$ and $1P_{e(h)}$ states also have minimal overlap in such large diameter quantum confined systems. Large diameter systems which minimize electron-phonon interaction are expected to have narrower density of states and are more suitable for studies attempting to observe a phonon bottleneck

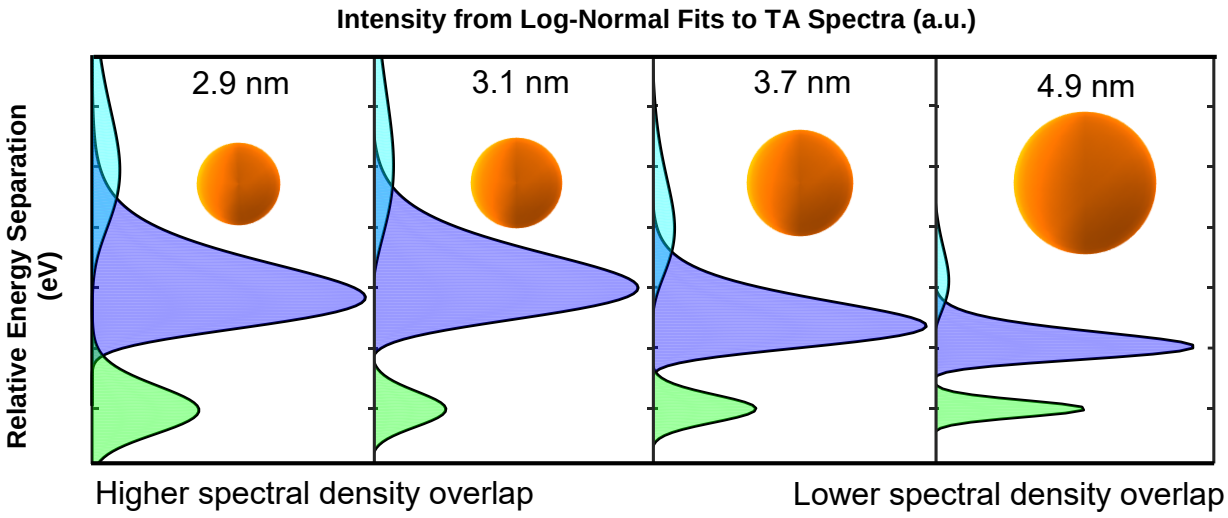


**Figure S24**. Experimentally obtained spectral density for 2.9 nm, 3.1 nm, 3.7 nm and 4.9 nm oleate capped PbS QD solutions for The lineshapes and intensities were obtained directly from fits to the transient absorption spectra. The 1S state energies (green) were set to 0 eV along the y-axis while the 1P (violet) and 1D (cyan) states remained unchanged, maintaining their respective energy separations from the 1S state.

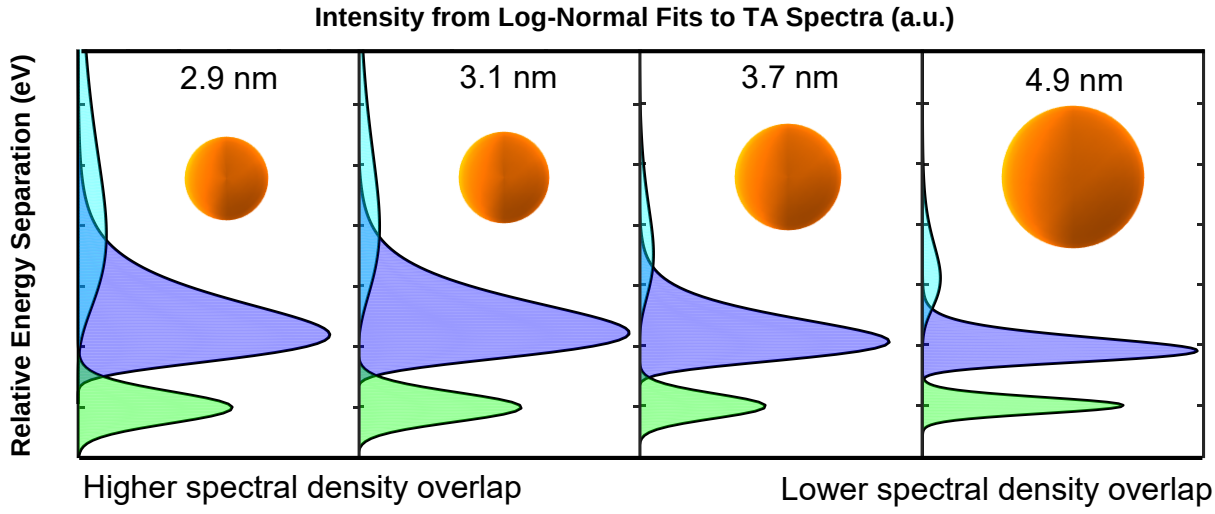


**Figure S25**. Experimentally obtained spectral density for 2.9 nm, 3.1 nm, 3.7 nm and 4.9 nm $I^-$/MPA capped PbS QD films. The lineshapes and intensities were obtained directly from fits to the transient absorption spectra. The 1S state energies (green) were set to 0 eV along the y-axis while the 1P (violet) and 1D (cyan) states remained unchanged, maintaining their respective energy separations from the 1S state.

**References:**


(1) Efros, A.; Efros, A. L., Interband Light Absorption in Semiconductor Spheres. *Sov. Phys. Semicond.* **1982,** *16,* 772-775.
(2) Kang, I.; Wise, F. W., Electronic Structure and Optical Properties of PbS and PbSe Quantum Dots. *J. Opt. Soc. Am. B* **1997,** *14,* 1632-1646.
(3) Crisp, R. W.; Kroupa, D. M.; Marshall, A. R.; Miller, E. M.; Zhang, J.; Beard, M. C.; Luther, J. M., Metal Halide Solid-State Surface Treatment for High Efficiency PbS and PbSe Qd Solar Cells. *Sci. Rep.* **2015,** *5,* 9945.
(4) Chernomordik, B. D.; Marshall, A. R.; Pach, G. F.; Luther, J. M.; Beard, M. C., Quantum Dot Solar Cell Fabrication Protocols. *Chem. Mater.* **2016,** *29,* 189-198.
(5) Grieco, C.; Kennehan, E. R.; Rimshaw, A.; Payne, M. M.; Anthony, J. E.; Asbury, J. B., Harnessing Molecular Vibrations to Probe Triplet Dynamics During Singlet Fission. *J. Phys. Chem. Lett.* **2017,** 5700-5706.
(6) Klimov, V. I.; Mikhailovsky, A. A.; McBranch, D. W.; Leatherdale, C. A.; Bawendi, M. G., Mechanisms for Intraband Energy Relaxation in Semiconductor Quantum Dots: The Role of Electron-Hole Interactions. *Phys. Rev. B* **2000,** *61,* R13349-R13352.
(7) Klimov, V. I., Optical Nonlinearities and Ultrafast Carrier Dynamics in Semiconductor Nanocrystals. *J. Phys. Chem. B* **2000,** *104,* 6112-6123.
(8) Klimov, V.; Hunsche, S.; Kurz, H., Biexciton Effects in Femtosecond Nonlinear Transmission of Semiconductor Quantum Dots. *Phys. Rev. B* **1994,** *50,* 8110-8113.
(9) Zhang, J.; Jiang, X., Steady State Photoinduced Absorption of Pbs Quantum Dots Film. *Appl. Spec. Lett.* **2008,** *92,* 141108.
(10) Luther, J. M.; Jain, P. K.; Ewers, T.; Alivisatos, A. P., Localized Surface Plasmon Resonances Arising from Free Carriers in Doped Quantum Dots. *Nat. Mater.* **2011,** *10,* 361-366.
(11) Munson, K. T.; Grieco, C.; Kennehan, E. R.; Stewart, R. J.; Asbury, J. B., Time-Resolved Infrared Spectroscopy Directly Probes Free and Trapped Carriers in Organo-Halide Perovskites. *ACS Energy Lett.* **2017,** *2,* 651-658.
(12) Tang, J.; Kemp, K. W.; Hoogland, S.; Jeong, K. S.; Liu, H.; Levina, L.; Furukawa, M.; Wang, X.; Debnath, R.; Cha, D., et al., Colloidal-Quantum-Dot Photovoltaics Using Atomic-Ligand Passivation. *Nat. Mater.* **2011,** *10,* 765-771.
(13) Jeong, K. S.; Tang, J.; Liu, H.; Kim, J.; Schaefer, A. W.; Kemp, K. W.; Levina, L.; Wang, X.; Hoogland, S.; Debnath, R., et al., Enhanced Mobility-Lifetime Products in PbS Colloidal Quantum Dot Photovoltaics. *ACS Nano* **2011,** *6,* 89-99.
(14) Hillhouse, H. W.; Beard, M. C., Solar Cells from Colloidal Nanocrystals: Fundamentals, Materials, Devices, and Economics. *Curr. Opin. Coll. & Interface Sci.* **2009,** *14,* 245-259.
(15) Krauss, T. D.; Wise, F. W.; Tanner, D. B., Observation of Coupled Vibrational Modes of a Semiconductor Nanocrystal. *Phys. Rev. Lett.* **1996,** *76,* 1376-1379.
(16) Etchegoin, P. G.; Cardona, M.; Lauck, R.; Clark, R. J. H.; Serrano, J.; Romero, A. H., Temperature-Dependent Raman Scattering of Natural and Isotopically Substituted PbS. *Phys. State. Sol.* **2007,** *245,* 1125-1132.
(17) Krauss, T. D.; Wise, F. W., Raman-Scattering Study of Exciton-Phonon Coupling in PbS Nanocrystals. *Phys. Rev. B.* **1997,** *55,* 9860-9865.
(18) Riesen, H.; Wiebeler, C.; Schumacher, S., Optical Spectroscopy of Graphene Quantum Dots: The Case of C132. *J. Phys. Chem. A* **2014,** *118,* 5189-5195.

(19) Goupalov, S. V., Selection Rules for Optical Transitions in PbSe Nanocrystal Quantum Dots: Drastic Effect of Structure Inversion Asymmetry. *Phys. Rev. B* **2009,** *79*.
(20) Gellen, T. A.; Lem, J.; Turner, D. B., Probing Homogeneous Line Broadening in CdSe Nanocrystals Using Multidimensional Electronic Spectroscopy. *Nano Lett.* **2017,** *17*, 2809-2815.
(21) Gilmore, R. H.; Lee, E. M.; Weidman, M. C.; Willard, A. P.; Tisdale, W. A., Charge Carrier Hopping Dynamics in Homogeneously Broadened PbS Quantum Dot Solids. *Nano Lett.* **2017,** *17*, 893-901.
(22) Nomura, S.; Kobayashi, T., Exciton–Lo-Phonon Couplings in Spherical Semiconductor Microcrystallites. *Phys. Rev. B* **1992,** *45*, 1305-1316.
(23) Takagahara, T., Electron-Phonon Interactions and Excitonic Dephasing in Semiconductor Nanocrystals. *Phys. Rev. Lett.* **1993,** *71*, 3577-3580.